The Unexpected Optical and Ultraviolet Variability of the Standard Star α Sex (HD 87887)

Richard Monier[1] , Dominic M. Bowman[2] , Yveline Lebreton[1,3] , and Morgan Deal[1,4]

[1] LESIA, UMR 8109, Observatoire de Paris et Université Pierre et Marie Curie Sorbonne Universités, place J. Janssen, Meudon, France; Richard.Monier@obspm.fr
[2] Institute of Astronomy, KU Leuven, Celestijnenlaan 200D, B-3001 Leuven, Belgium
[3] Univ Rennes, CNRS, IPR (Institut de Physique de Rennes) - UMR 6251, F-35000 Rennes, France
[4] Instituto de Astrofísica e Ciências do Espaço, Universidade do Porto, CAUP, Rua das Estrelas, PT4150-762 Porto, Portugal

Abstract

The analysis of the available Transiting Exoplanet Survey Satellite (TESS) light curves of α Sex (HD 87887) reveals low-frequency pulsations with a period of about 9.1 hr in this spectroscopic A0 III standard star. The IUE observations in 1992 December reveal large flux variations both in the far-UV and in the mid-UV, which are accompanied by variations of the brightness in the V band recorded by the the Fine Error Sensor on board IUE. The ultraviolet variability could be due to an eclipse by an hitherto undetected companion of smaller radius, possibly $2.5 R_\odot$, but this needs confirmation by further monitoring possibly with TESS. An abundance determination yields solar abundances for most elements. Only carbon and strontium are underabundant and titanium, vanadium, and baryum mildly overabundant. Identification is provided for most of the lines absorbing more than 2% in the optical spectrum of α Sex. Stellar evolution modeling shows that α Sex is near the terminal-age main sequence, and its mass, radius, and age are estimated to be $M = 2.57 \pm 0.32 M_\odot$, $R = 3.07 \pm 0.90 R_\odot$, $A = 385 \pm 77$ Myr, respectively.

Unified Astronomy Thesaurus concepts: A giant stars (4)

Supporting material: machine-readable table

1. Introduction

Although α Sex is a bright and standard A0 III giant (Gray & Garrison 1987), it has not been extensively studied for a star of its brightness: only 91 references can be found in SIMBAD.[5] The most recent abundance analysis is that of Pintado & Adelman (2003) who used optical spectra and derived abundances for 19 elements. They found mostly solar abundances including helium. The only species that deviated from solar abundances are scandium, which is underabundant, sulfur, and calcium marginally underabundant, manganese marginally overabundant, and barium overabundant. A new determination of the iron abundance was made by Adelman (2014) who found a slight underabundance.

Among intermediate-mass main-sequence stars of spectral type A and F, the most common type of pulsator are the δ Sct stars. These stars have low-radial-order pressure modes with periods of order of hours that are excited by a heat-engine mechanism (Breger 2000). Approximately 50% of main-sequence A and early-F stars are δ Sct stars based on modern high-precision space photometry (Murphy et al. 2019; Bowman & Kurtz 2021). The identification of modeling of stellar pulsations, known as asteroseismology (Aerts et al. 2010), yields important constraints on the physical processes at work within stars such as rotation, mixing, and atomic diffusion. Therefore, the identification of high-quality pulsating stars is essential for follow-up modeling.

In this paper, we report on work based on new high-precision light curves from the NASA Transiting Exoplanet Survey Satellite (TESS) mission (Ricker et al. 2015) and on a new abundance analysis. The TESS light curve reveals that α Sex is a variable star with multiperiodic pulsations and periods of the order of several hours. The IUE archival observations of α Sex over 3 days in 1992 December are also analyzed.

This article is organized as follows. Section 2 describes the TESS light curves of α Sex and their analysis, Section 3 the analysis of the IUE spectra, and Section 4 the abundance determinations for 19 chemical elements. In Section 5, we use the SPInS stellar parameter inference program (Lebreton & Reese 2020) and the BaSTI-IAC grid of stellar models (Hidalgo et al. 2018) to derive the evolutionary status, mass, radius, and age of α Sex. We discuss the nature of α Sex and conclude in the final section.

2. The TESS Light Curves of α Sex and Their Analysis

The TESS mission observed α Sex in sectors 8, 35 and 45 in its short cadence (i.e., 2 minutes) mode. We retrieved both the simple aperture photometry (SAP) and predata search conditioning (PDC-SAP) 2 minute light curves from the Mikulski Archive for Space Telescopes[6], which are extracted from the target pixel files using NASA's SPOC pipeline (see Jenkins et al. 2016 for details). Since α Sex is a relatively bright star for the TESS mission, it is moderately saturated in its target pixel files. However, the aperture mask assigned by the SPOC pipeline includes sufficient pixels, which includes the short bleed columns, to extract a light curve. In such cases, TESS light curves are more than adequate at detecting and characterizing pulsating stars (see, e.g., Bowman et al. 2022).

---

[5] http://simbad.u-strasbg.fr/simbad/
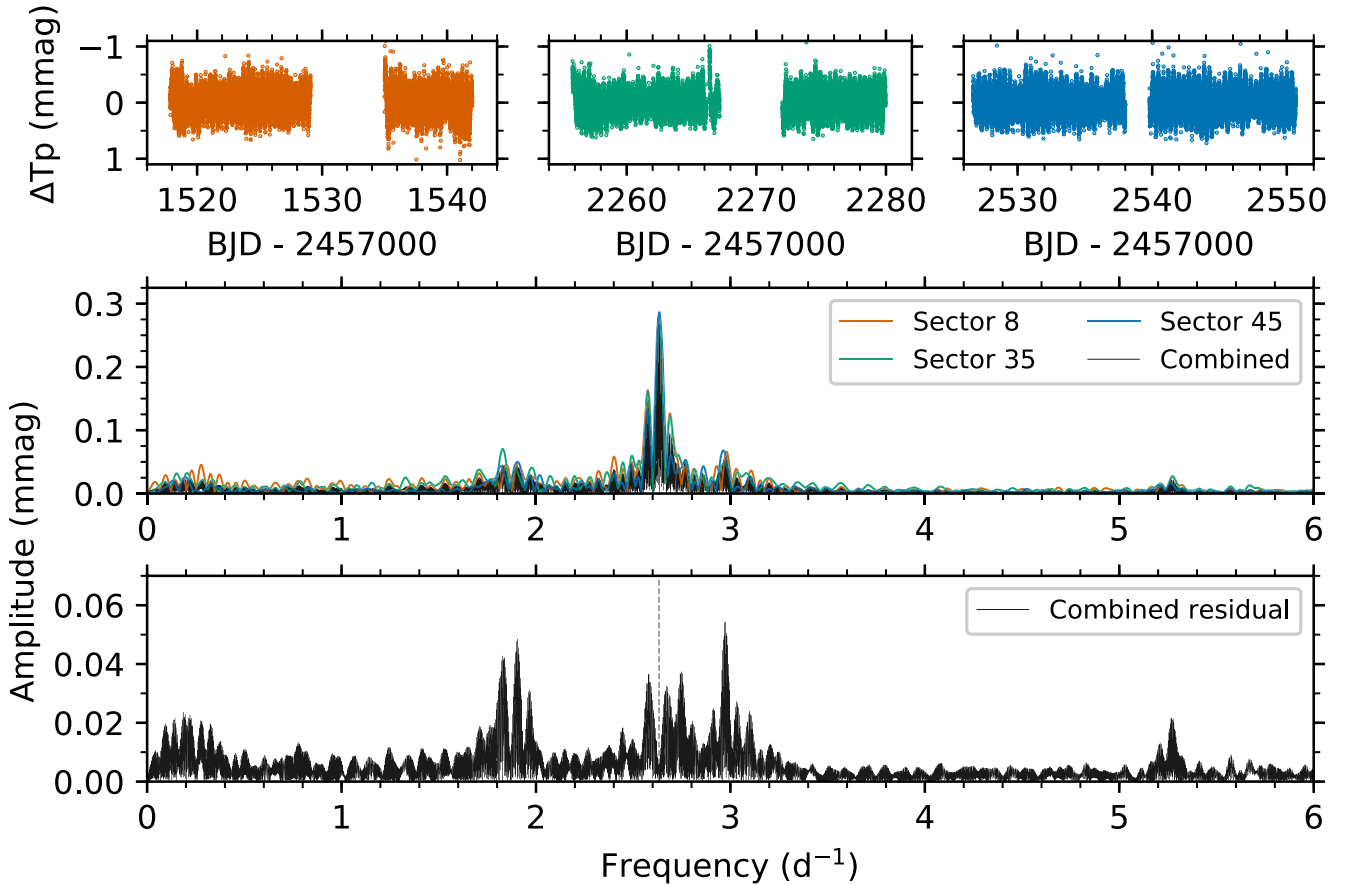
---

[6] https://archive.stsci.edu/

Figure 1. Top panels: TESS light curves for sectors 8, 35, and 45. Middle panel: amplitude spectra of each TESS sector and all three sectors combined. Bottom panel: residual amplitude spectrum of all three combined sectors after the dominant frequency has been removed.

We checked for possible sources of contamination, but could not verify any known and sufficiently bright background or nearby sources. Using the LIGHTKURVE software (Lightkurve collaboration et al. 2018) software in combination with Gaia astrometry (Gaia Collaboration 2020), there are a only a few very faint (Gaia $G > 14$ mag) sources located within the assigned target pixel aperture mask, hence their flux contribution is negligible.

Given the large gaps between the sectors 8, 35, and 45 light curves, we opted to analyze them separately for signatures of pulsations to avoid issues arising from the complex spectral window pattern in a combined light curve. Each TESS sector light curve maximally spans approximately 24 days with varying duty cycles depending on the specific sector. This yields a resultant frequency resolution following the Rayleigh criterion of approximately 0.042 day^{-1} for an individual sector. We converted the extracted PDC-SAP 2 minute light curves to have units of magnitudes and show them in Figure 1. We calculated discrete Fourier transforms (Kurtz 1985) and show the resultant amplitude spectra for each sector and the combined sectors 8, 35, and 45 light curve in the middle panel of Figure 1. A dominant frequency of 2.63 day^{-1}, corresponding to a period of 9.1 hr, is apparent in the amplitude spectra of all three individual light curves. Additional multiperiodic variability is present in the frequency range of 1.8 day^{-1} up to 5.3 day^{-1}, with amplitudes ranging up 0.3 mmag.

We performed iterative prewhitening to extract significant frequencies for each of the three individual TESS sectors. Significant frequencies are those that have an amplitude signal-to-noise ratio (S/N) of $\geqslant 5$, in which the noise is calculated using a symmetric local window centered at the location of the extracted frequency in the residual amplitude spectrum (Bowman & Michielsen 2021). In our frequency analysis of the individual TESS sectors, two significant frequencies are extracted: the dominant frequency and a second indistinguishable for its harmonic given the low resolving power of a single TESS sector. Specifically in sector 45, however, several additional frequencies are detected within the frequency regime of the dominant frequency. This is not the signature of rotational modulation, but in fact is evidence of multiperiodic pulsations. Moreover, for such a frequency to be caused by rotational modulation, this implies an extremely rapid rate of surface rotation, which we deem unlikely given the known projected surface rotation rate from spectroscopy $v_e \sin i = 21$ km s^{-1} (Abt et al. 2002).

We provide the list of significant frequencies for each sector, which were optimized using a multi-frequency nonlinear least-squares fit to the light curve (Bowman & Michielsen 2021), in Table 1. In the bottom panel of Figure 1, we show the residual amplitude spectrum after the dominant frequency has been optimized and removed from the combined sectors 8, 35, and 45 light curve. This clearly demonstrates the multiperiodic variability of α Sex between 1.8 and 5.3 days^{-1}, which is

Table 1
Frequencies, Amplitudes, and Phases of the Significant Pulsation Modes in α Sex, and Their 1σ Uncertainties Calculated from a Nonlinear Least-squares Fit to the Light Curve

Frequency (day^{-1})	Amplitude (mmag)	Phase (rad)
Sector 8		
2.6313 ± 0.0001	0.280 ± 0.002	0.221 ± 0.007
5.2745 ± 0.0017	0.024 ± 0.002	-2.727 ± 0.083
Sector 35		
2.6333 ± 0.0001	0.271 ± 0.002	1.157 ± 0.007
5.2753 ± 0.0013	0.028 ± 0.002	-0.863 ± 0.063
Sector 45		
1.8139 ± 0.0008	0.0409 ± 0.002	-1.042 ± 0.034
1.9054 ± 0.0006	0.0537 ± 0.002	2.279 ± 0.026
2.5791 ± 0.0009	0.0612 ± 0.002	-2.150 ± 0.031
2.6329 ± 0.0004	0.2800 ± 0.002	2.290 ± 0.010
2.6826 ± 0.0042	0.0316 ± 0.002	-3.017 ± 0.081
2.7382 ± 0.0019	0.0407 ± 0.002	0.714 ± 0.041
2.9678 ± 0.0005	0.0621 ± 0.002	1.156 ± 0.023
3.0987 ± 0.0014	0.0231 ± 0.002	3.046 ± 0.062
5.2634 ± 0.0018	0.0167 ± 0.002	1.347 ± 0.082

affected by the complex spectral window pattern resulting from the combined light curves.

3. The Ultraviolet Variability of α Sex

Nine high resolution SWP and LWP spectra of α Sex were obtained with the International Ultraviolet Explorer from 1992 December 24 to 27 through the large apertures in the frame of program NA026 (PI: Richard Monier). These spectra are calibrated into absolute fluxes, their resolving power is about 25,000 and their S/N is typically a 10–20. They were retrieved from the Mikulski Archive for Space Telescope,[7] they are collected in Table 2

These spectra have been degraded to a lower resolution of about 7 Å comparable to the IUE low resolution in order to highlight the variations. The large variations in the far and mean ultraviolet are shown in Figure 2. In the far-UV, four pseudo continuuum windows (regions free of strong lines) are present at 1284, 1342, 1457, and 1756 Å. The ratio of maximum (SWP 46599) to minimum flux (SWP 46577) is about the same in these three windows: 1.35 ± 0.03. In the mean UV, two windows are observed at 2047 and 2650 Å, where the ratio is about 1.38 ± 0.01, discarding the spectrum with very low flux LWP 24589. Including this spectrum, the ratio becomes 44 at 2047 Å and 57 at 2650 Å. Before each of these observations, the brightness of α Sex was monitored with the Fine Error Sensor (FES) in a broad spectral band near 5000 Å. The FES counts do follow the UV flux variations: they are larger on December 27 (around 5450 counts), minimum on December 25 (around 3270 counts), and intermediate on December 24 (around 3690 counts), which means that the UV flux varied in phase with the brightness of the star at 5000 Å. At ultraviolet maximum, the lines in SWP 46599 are consistently redshifted by about 13.7 km s^{-1} with respect to the spectrum at FUV minimum SWP 46577.

The large diming of the flux by about 70 % at minimum in the far-UV compared to the maximum flux could be due to a partial eclipse of α Sex by an hitherto undetected companion. The duration of the eclipse and the shape of the light curve are poorly constrained with the available data, it is therefore difficult to derive information on the radii, temperatures, and masses. We can crudely estimate the radius of the secondary star by using the relationship between the flux decrease:

$$\frac{f_{\min}}{f_{\max}} = \left(\frac{R_B}{R_A} \right)^2 \tag{1}$$

and the radii R_A of α Sex and R_B of the putative companion. Assuming a radius of about 3.0 $R_\odot$ for R_A (see Section 3), this yields a radius R_B close to 2.5 $R_\odot$. If the system is indeed eclipsing, it is seen edge-on ($i = \frac{\pi}{2}$). We can estimate a rotation period of 7 days and 19 hr by using the projected equatorial velocity and the estimated radius in Section 6 where we discuss the evolutionary status of α Sex. Since no eclipse is seen in the current TESS data, we can place a lower limit on the orbital period of about 28 days, which means that the semimajor axis of the ellipse must be large. Eggleton & Tokovinin (2008) mentioned that α Sex could be a binary, presumably with a long period. Kervella et al. (2019) also think that α Sex may be a binary system considering the renormalized unit weight error from Gaia DR2. Note that the large ultraviolet variations we observe for α Sex do not resemble those of δ Scuti observed by Monier (1991) throughout its pulsation cycle. The ultraviolet variations of δ Scuti have modest amplitudes which increase toward shorter wavelengths as expected for a change in effective temperature during the pulsation cycle. This is not the trend we observe for α Sex for which the amplitude of the flux variations does not increase toward shorter wavelengths (the far and mid-UV fluxes vary by a similar amount with time).

4. The Abundance Pattern of α Sex

4.1. Observations

Four I high resolution profiles ($R = 65,000$) of α Sex have been fetched from the Polarbase archive.[8] These profiles were acquired on 2018 May 10 with the spectropolarimeter NARVAL (Petit et al. 2014) installed at the 2 m TBL at Pic du Midi Observatory. NARVAL is a cross-dispersed échelle spectrograph mounted on a bench and fed with a fiber from a Cassegrain-mounted polarimeter unit with a wavelength coverage of 3690 up to 10,480 Å. The individual I profiles which have a S/N of 200 around 5000 Å were coadded into a mean spectrum of S/N of 350. This final spectrum has been sliced into 200 Å wide intervals which were then normalized to a continuum by fitting a cubic spline through narrow regions free of absorption lines.

4.2. Fundamental Parameters

The effective temperature (T_{eff}) and surface gravity (log g) of α Sex were determined using the UVBYBETA code developed by Napiwotzki et al. (1993). This code is based on the Moon & Dworetsky (1985) grid, which calibrates the $uvby\beta$ photometry in terms of T_{eff} and log g. The photometric data was taken from Hauck & Mermilliod (1998). The derived effective temperature is $T_{\mathrm{eff}} = 9950 \pm 125$ K and

Table 2
Log of IUE Observations

Spectrum	Observation Date	Resolution	Observation Time	Exposure Time (s)	FES Counts
SWP 46576	1992-12-24	High	13:47:20	390	3587
LWP 24572	1992-12-24	High	13:59:05	180	3696
SWP 46577	1992-12-24	High	16:12:40	1200	3632
LWP 24573	1992-12-24	High	16:27:19	390	3841
SWP 46584	1992-12-25	High	15:56:55	1200	3321
LWP 24589	1992-12-25	High	16:25:57	4200	3227
SWP 46598	1992-12-27	High	10:14:56	1800	5407
LWP 24605	1992-12-27	Low	11:05:42	420	5542
LWP 24606	1992-12-27	High	12:50:53	420	5443
SWP 46599	1992-12-27	High	16:46:54	600	5401

$\log g = 3.60 \pm 0.25$ dex, respectively (see Section 4.2 in Napiwotzki et al. 1993). This value is in good agreement with previous determinations: Adelman (2014) derived $T_{\mathrm{eff}} = 9875$ K from spectrophotometry and the fit to the H_{γ} line; McDonald et al. (2012) derived $T_{\mathrm{eff}} = 9984$ K by comparing the spectral energy distribution of α Sex to model atmospheres; and Pintado & Adelman (2003) derived $T_{\mathrm{eff}} = 950$ K from calibration of uvbyβ photometry.

4.3. Abundance Determination

4.3.1. Model Atmospheres and Spectrum Synthesis

The ATLAS9 code (Kurucz 1992) was used to compute a first model atmosphere for the effective temperature and surface gravity of α Sex assuming a plane parallel geometry, a gas in hydrostatic and radiative equilibrium and local thermodynamical equilibrium. The ATLAS9 model atmosphere contains 72 layers with a regular increase in $\log \tau_{\mathrm{Ross}} = 0.125$ and was calculated assuming a solar chemical composition (Grevesse & Sauval 1998). It was converged up to $\log \tau = -5.00$ in order to attempt reproduce the cores of the Balmer lines. This ATLAS9 version uses the new opacity distribution function of Castelli & Kurucz (2003) computed for that solar chemical composition. Once a first set of elemental abundances was derived using the ATLAS9 model atmosphere, the atmospheric structure was recomputed for these abundances using the Opacity sampling ATLAS12 code (Kurucz 2005, 2013). New slightly different abundances were then derived and a new ATLAS12 model recomputed until the abundances of iteration (n-1) differed of those of iteration (n) by less than ± 0.10 dex.

The abundances of nineteen chemical elements have been derived by iteratively adjusting synthetic spectra to the normalized spectra and looking for the best fit to carefully selected unblended lines. Specifically, synthetic spectra were computed assuming LTE using Hubeny & Lanz (1992) SYNSPEC49 code which computes lines for elements up to $Z = 99$. The synthetic spectra were further convolved with a rotation parabolic profile for $v_e \sin i = 21$ km s^{-1} (Abt et al. 2002) and the appropriate FWHM of the instrumental profile of NARVAL. The projected equatorial velocity has been checked by modeling the Fe II lines in the range 4500–4550 Å, they all yield a $v_e \sin i$ of about 20.0 ± 1.0 km s^{-1}, which agrees well with the value provided by Royer et al. (2002). In order to derive the microturbulent velocity of α Sex, we simultaneously derived the iron abundance [Fe/H] for 50 unblended Fe II lines and a set of microturbulent velocities ranging from 0.0 to 2.0

km s^{-1}. The adopted microturbulent velocity, $\xi_t = 1.5$ km s^{-1}, minimizes the standard deviations, i.e., for that value all Fe II lines yield a similar iron abundance.

We used only unblended lines to derive the abundances. A grid of synthetic spectra was computed with SYNSPEC49 (Hubeny & Lanz 1992) to model each selected unblended line of the nineteen elements for α Sex. For each modeled transition, the adopted abundance is that which provided the best fit calculated with SYNSPEC49 to the observed normalized profile. Computations were iterated varying the unknown abundance until minimization of the χ^2 between the observed and synthetic spectrum was achieved over the spectral range limited to ± 1.5 Å from the line center. The selected lines are well separated from their neighbors allowing to place the continuum properly on both wings of the line. For a given element, the final abundance is a weighted mean of the abundances derived for each transition (the weights are derived from the NIST grade assigned to that particular transition).

5. Abundance Determinations and Line Identifications for α Sex

The determined abundances for α Sex, expressed relative to hydrogen as $\log(n_X) - 12.0$ (adopting $\log(n_H) = 12.0$) and their errors (standard deviations) are collected in Table 3. Solar abundances are taken from Grevesse et al. (2007). We find that the abundances of α Sex are close to the solar composition.

Helium, nitrogen, oxygen, magnesium, aluminum, silicon, phosphorus, sulfur, calcium, scandium, chromium, manganese, iron, and nickel have solar abundances. Only carbon and strontium are underabundant. Titanium, vanadium, and baryum are mildly overabundant. The final synthetic spectrum allows to identify most of the lines, which absorb more than 2% of the local continuum. It is compared to the observed spectrum in the range 4500–4550 Å in Figure 3. The identifications of these lines are collected in Table 4 where E_{low} is the energy of the lower excitation level involved in the transition.

6. The Evolutionary Status of α Sex

6.1. Estimations of Mass, Radius, and Evolutionary Stage

To estimate the mass, radius, and age of the star, we used the SPInS stellar model optimization tool (Lebreton & Reese 2020). SPInS uses a Bayesian approach to find the probability distribution function of stellar parameters from a set of constraints. At the heart of the code is a Markov chain Monte Carlo sampler coupled with interpolation within a precomputed stellar model grid. Here, we used the BaSTI-IAC grid of stellar
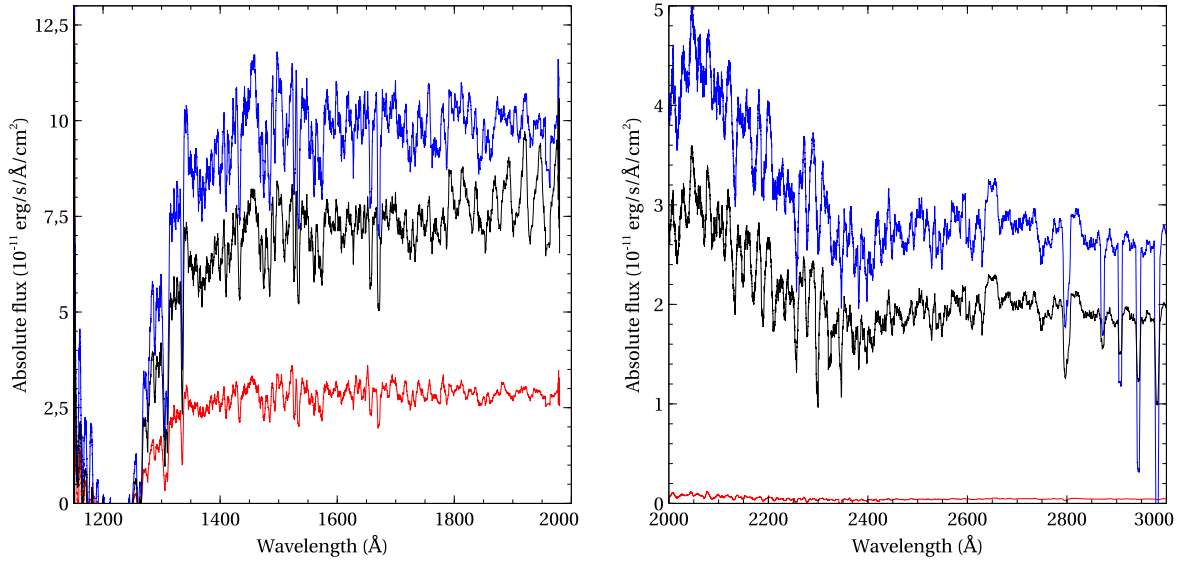
Figure 2. Left: the far-UV flux variations of α Sex (SWP 46599, FUV max in blue; SWP 46577 FUV min in red), Right: the mid-UV flux variations (LWP 24606: mid-UV max in blue; LWP2 4589: mid-UV min in red).

Table 3
Elemental Abundances and Their Errors for α Sex

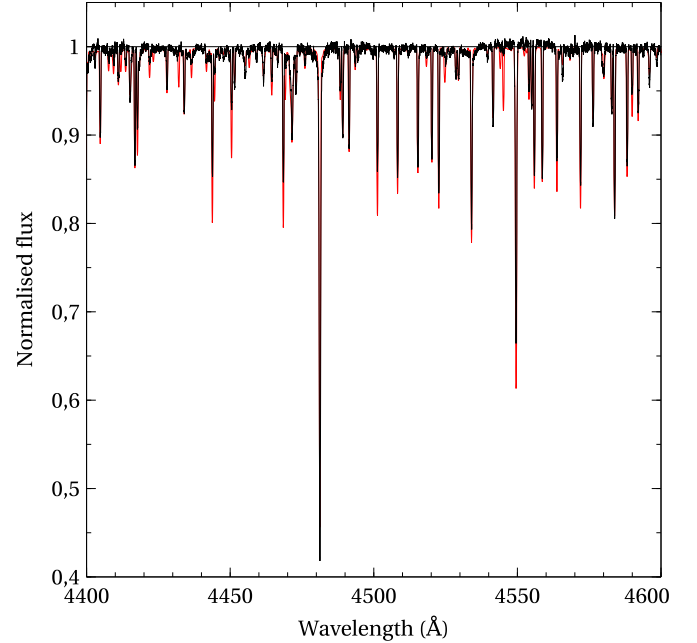| Element	Solar Abundance	Absolute Abundance	Error
He	−1.07	−1.07	0.32
C	−3.61	−3.37	0.09
N	−4.22	−4.39	0.20
O	−3.34	−3.31	0.19
Mg	−4.47	−4.50	0.08
Al	−5.63	−5.37	0.20
Si	−4.49	−4.49	0.18
P	−6.64	−6.64	0.16
S	−4.86	−4.86	0.11
Ca	−5.69	−5.71	0.05
Sc	−8.83	-9.10	0.28
Ti	−7.10	−6.80	0.13
V	−8.00	−7.60	0.08
Cr	−6.36	−6.36	0.05
Mn	−6.61	−6.57	0.11
Fe	−4.55	−4.69	0.10
Ni	−5.97	−5.99	0.13
Sr	−9.08	−9.23	0.09
Ba	−9.83	−9.34	0.19

Figure 3. Comparison of the observed mean spectrum of HD 87887 (in black) and the synthetic spectrum (in red) in the range 4500–4550 Å.

models (Hidalgo et al. 2018). This grid is for a solar-scaled heavy element distribution with the solar mixture taken from Caffau et al. (2011) complemented by Lodders (2010), which corresponds to $(Z/X)_\odot = 0.0209$. The grid considers convective core overshooting included as an instantaneous mixing between Schwarzschild's convective limit up to layers at a distance $\alpha_{ov} = 0.2 H_P$ from it, where H_P is the pressure scale height at the Schwarzschild limit. Microscopic diffusion is not taken into account. In the calculation process, SPInS can incorporate various priors on the initial mass function (IMF), stellar-formation rate (SFR), and metallicity distribution function (MDF). Here we took Kroupa et al. (2013) as IMF and no priors on the SFR and MDF.

With the observational constraints for HD 87887 derived in Sections 4 and 5 ($T_{eff} = 9950 \pm 125$ K, log $g = 3.60 \pm 0.25$ dex and [Fe/H] $= -0.14 \pm 0.10$), SPInS provided as mean values an age $A = 385 \pm 77$ Myr, a mass $M = 2.57 \pm 0.32 M_\odot$,

a radius $R = 3.07 \pm 0.90 R_\odot$, a mean density $\bar{\rho} \simeq 0.13 \pm 0.11$ g cm^{-3}, and a luminosity $L = 90 \pm 52 L_\odot$. The observed position of the star in the Kiel diagram is provided in Figure 4 together with the isochrones for the $\pm 1\sigma$ age values inferred by SPInS showing that the star evolves at the vicinity of the main-sequence turn-off. We can compare the inferred radius with the observed one using the Swihart et al. (2017)'s angular diameter obtained by interferometry, $\theta \simeq 0.361 \pm 0.065$ mas, and parallax values from the literature, that is $\varpi_G = 7.66 \pm 0.37$ mas (Gaia Collaboration 2020; Gaia DR3) and $\varpi_H = 11.51 \pm 0.98$ mas (van Leeuwen 2007; Hipparcos). This leads to linear radius values of $R_G \simeq 5.1 \pm 1.2 R_\odot$ and $R_H \simeq 3.4 \pm 0.9 R_\odot$, respectively, such that R_H is closer to our inferred radius rather than R_G. To assess our results, we also attempted
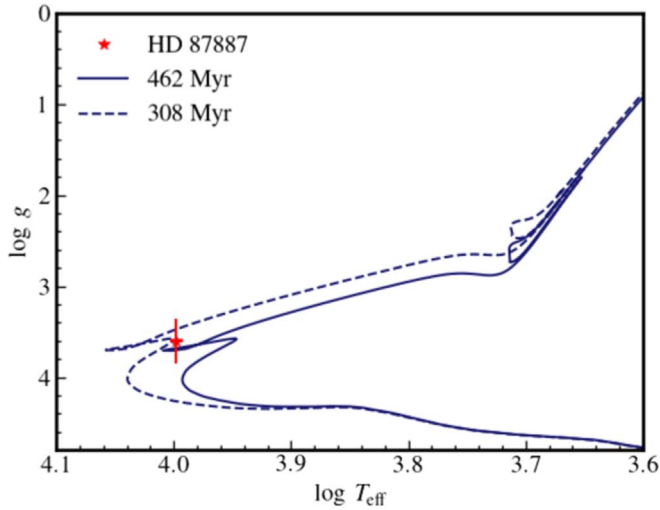
Figure 4. Kiel diagram showing the observed position of HD 87887 together with two isochrones computed for the $\pm 1\sigma$ age values inferred by SPInS

to derive the stellar parameters using absolute magnitude and a color index in SPInS instead of the T_{eff} and $\log g$ values derived previously. From the Hipparcos and Tycho-2 constraints on ϖ_H, $V_T = 4.474 \pm 0.003$ mag and $(B - V)_T = -0.030 \pm 0.004$ mag (Høg et al. 2000), we found an age $A = 350 \pm 25$ Myr, a mass $M = 2.87 \pm 0.12\,M_\odot$, and a radius $R = 3.66 \pm 0.34\,R_\odot$, all compatible with our results. On the other hand, we could not find a solution when using the absolute Gaia G-magnitude and (BP-RP) color index, which may indicate difficulties with the Gaia parallax. Indeed, the Gaia-DR3 parallax of α Sex should be taken with care for three reasons: (i) the star is bright; (ii) the astrometric excess noise of the source is around 2 mas;[9] and (iii) it is a member of a binary system (Kervella et al. 2019).

7. Discussion and Conclusions

To place the detected variability caused by pulsations in an evolutionary context, we calculate the expected period of the fundamental radial pressure mode of α Sex using its derived parameters. Following Ledoux (1945), we estimate the period of the fundamental radial pressure mode of α Sex to be:

$$P = \left(\frac{3\pi}{G\bar{\rho}} \times \frac{1}{3\Gamma_1 - 4} \right)^{\frac{1}{2}}, \quad (2)$$

assuming the adiabatic exponent is constant throughout the star. For an ideal monoatomic gas for which $\Gamma_1 \approx 5/3$, this yields $\nu = 2.6 \pm 1.1$ day^{-1} (i.e., $P = 9.3 \pm 4.1$ hr). This estimate is analogous and compatible with that of the empirical $Q = P\sqrt{\frac{\rho}{\rho_\odot}}$ relation for radial pressure modes in δ Sct stars (Breger & Bregman 1975), in which $Q = 0.033$ for fundamental radial pressure modes. Our estimates are entirely consistent with the observed dominant frequency in the TESS light curve of α Sex. Therefore, we conclude that the observed variability is low-radial order p-mode pulsations. Given its advanced evolutionary stage, it is possible that the observed pulsation modes are of mixed pressure- and gravity-mode

character (Aerts et al. 2010). However, future forward asteroseismic data based on much longer light curves with higher duty cycle are needed to confirm this.

Although the pulsations observed in the TESS light curve of α Sex may at first glance appear to resemble the frequency spectra of slowly pulsating B (SPB) stars (e.g., Bowman et al. 2019; Sharma et al. 2022), we present several reasons why this is not the case. SPB stars are mid-to-late B-type-dwarf stars and hence hotter and less evolved than α Sex. Moreover, SPB stars are typically fast rotators (Pedersen et al. 2021) and α Sex is not. Indeed, α Sex does not have the characteristic flat-bottomed Fe II lines that Vega has, which is a fast rotator seen pole-on (Hill et al. 2010). If, for example, α Sex were an SPB star and lies within an extension of the SPB stars toward cooler temperatures and lower gravities, it would need to be pulsating in gravity or perhaps Rossby modes (for which the restoring force is the Coriolis force) rather than pressure modes. However, the low $v \sin i$ combined with $i \simeq 90°$ given that the system is eclipsing based on the indicative UV photometry eclipse, makes α Sex unlikely to have gravito(inertial) modes. This is because the frequencies of slowly rotating SPB pulsators are not as high as 2.5 c d^{-1} as seen in the TESS light curve of α Sex (see e.g., Pedersen et al. 2021). For gravity-mode frequencies to be so high in such a star, the impact of the Coriolis force would also need to be large, thus α Sex would need to be rapidly rotating. Finally, gravity modes are unlikely to exist above the fundamental radial pressure mode frequency that we derive in this work. Hence we conclude low-radial order pressure and/or mixed modes are the most likely identification of the pulsations based on the fundamental parameters of α Sex derived in this work.

On the issue of whether pressure mode pulsations are expected in a star such as α Sex, we refer to Bowman & Kurtz (2021) and Murphy et al. (2019). In these studies of thousands of δ Sct stars observed by the Kepler space telescope, the observational hot edge of the classical instability strip was determined to correspond to $T_{eff} \simeq 9000$ K based on the density of such stars in the Kiel and HR diagrams. However, there exist a nonnegligible number of outliers with hotter T_{eff} values. Pulsation excitation models struggle to explain the observed pulsations in such stars, because the heat-engine (κ) mechanism is inefficient at these temperatures (Dupret et al. 2004). Indeed, other pulsation excitation mechanisms operate in delta Scuti stars. Antoci et al. (2014) and Antoci et al. (2019) describe the role of turbulent pressure in the excitation of pulsations in δ Scuti stars, but such a mechanism typically excites high-radial order and thus high-frequency pressure modes. The discovery of pressure modes in α Sex make it an interesting case study for follow-up asteroseismic modeling. Further monitoring with TESS may confirm the presence of eclipses too.

---

[9] See https://gea.esac.esa.int/archive/documentation/GDR2/Gaia_archive/chap_datamodel/sec_dm_main_tables/ssec_dm_gaia_source.html and https://www.cosmos.esa.int/web/gaia/science-performance (F. Arenou 2022, private communication).

Appendix
Supplementary Data Table

The line identifications for α Sex in this work are provided in Table 4.

Table 4
Line Identifications for α Sex

λ_{obs} (Å)	λ_{lab} (Å)	Species	$\log gf$	E_{low}	References
3900.44	3900.55	Ti II	−0.45	9118.260	VALD
3903.78	3903.76	Fe II	−1.49	60807.23	VALD
3905.97	3906.04	Fe II	−1.83	44929.549	VALD
3913.47	3913.47	Ti II	−0.53	8997.710	VALD
3914.56	3914.50	Fe II	−4.05	13474.411	VALD

(This table is available in its entirety in machine-readable form.)

ORCID iDs

Richard Monier https://orcid.org/0000-0002-0735-5512
Dominic M. Bowman https://orcid.org/0000-0001-7402-3852
Yveline Lebreton https://orcid.org/0000-0002-4834-2144
Morgan Deal https://orcid.org/0000-0001-6774-3587

References

Abt, H. A., Levato, H., & Grosso, M. 2002, ApJ, 573, 359
Adelman, S. J. 2014, PASP, 126, 505A
Aerts, C., Christensen-Dalsgaard, J., & Kurtz, D. W. 2010, Asteroseismology (Berlin: Springer)
Antoci, A., Cunha, M., Houdek, G., et al. 2014, ApJ, 796, 118A
Antoci, V., Cunha, M. S., Bowman, D. M., et al. 2019, MNRAS, 490, 4040
Bowman, D. M., Burssens, S., Pedersen, M. G., et al. 2019, NatAs, 3, 760
Bowman, D. M., & Kurtz, D. W. 2021, MNRAS, 476, 3169
Bowman, D. M., & Michielsen, M. 2021, A&A, 656, A158
Bowman, D. M., Vandenbussche, B., Sana, H., et al. 2022, A&A, 658, A96
Breger, M. 2000, in ASP Conf. Ser. 210, Delta Scuti and Related Stars, Reference Handbook and Proc. of the 6th Vienna Workshop in Astrophysics, ed. M. Breger & M. Montgomery (San Francisco, CA: ASP), 3
Breger, M., & Bregman, J. N. 1975, ApJ, 200, 343
Caffau, E., Ludwig, H.-G., Steffen, M., et al. 2011, SoPh, 268, 255
Castelli, F., & Kurucz, R. L. 2003, in IAU Symp. 210, Modelling of Stellar Atmospheres, ed. N. Piskunov, W. W. Weiss, & D. F. Gray (Cambridge: Cambridge Univ. Press), A20
Dupret, M. A., Grigahcène, A., Garrido, R., et al. 2004, A&A, 414, L17
Eggleton, P. P., & Tokovinin, A. A. 2008, MNRAS, 389, 869
Gaia Collaboration 2020, yCat, I/350
Gray, R. O., & Garrison, R. F. 1987, ApJS, 65, 581G
Grevesse, N., Asplund, M., & Sauval, A. J. 2007, SSRv, 130, 105
Grevesse, N., & Sauval, A. J. 1998, SSRv, 85, 174
Hauck, B., & Mermilliod, M. 1998, A&AS, 129, 433
Hidalgo, S. L., Pietrinferni, A., Cassisi, S., et al. 2018, ApJ, 856, 125
Hill, G., Gulliver, A. F., & Adelman, S. J. 2010, ApJ, 712, 250H
Høg, E., Fabricius, C., Makarov, V. V., et al. 2000, A&A, 355, L27
Hubeny, I., & Lanz, T. 1992, A&A, 262, 514
Jenkins, J. M., Twicken, J. D., McCauliff, S., et al. 2016, Proc. SPIE, 9913, 99133E
Kervella, P., Arenou, F., Mignard, F., & Thévenin, F. 2019, A&A, 623, 72K
Kroupa, P., Weidner, C., Pflamm-Altenburg, J., et al. 2013, in Planets, Stars and Stellar Systems. Galactic Structure and Stellar Populations, ed. T. D. Oswalt & G. Gilmore, Vol. 5 (Dordrecht: Springer), 115
Kurtz, D. W. 1985, MNRAS, 213, 773
Kurucz, R. L. 1992, RMxAA, 23, 45
Kurucz, R. L. 2005, MSAIS, 8, 14
Kurucz, R. L. 2013, ATLAS12: Opacity sampling model atmosphere program, Astrophysics Source Code Library, ascl:1303.024
Lebreton, Y., & Reese, D. R. 2020, A&A, 642, A88
Ledoux, P. 1945, ApJ, 102, 143
Lightkurve Collaboration, Cardoso, J. V. M., Hedges,, C., et al. 2018, Lightkurve: Kepler and TESS time series analysis in Python, Astrophysics Source Code Library, ascl:1812.013
Lodders, K. 2010, Principles and Perspectives in Cosmochemistry, Vol. 16 (Berlin: Springer), 379
McDonald, I., Zijlstra, A. A., & Boyer, M. L. 2012, MNRAS, 427, 343
Monier, R. 1991, AJ, 102, 234M
Moon, T. T., & Dworetsky, M. M. 1985, MNRAS, 217, 315
Murphy, S. J., Hey, D., Van Reeth, T., & Bedding, T. R. 2019, MNRAS, 485, 2380
Napiwotzki, R., Schoenberner, D., & Wenske, V. 1993, A&A, 268, 653
Pedersen, M. G., Aerts, C., Pápics, P. I., et al. 2021, NatAs, 5, 715
Petit, P., Louge, T., Théado, S., et al. 2014, PASP, 126, 469P
Pintado, O., & Adelman, S. 2003, A&A, 406, 987P
Ricker, G. R., Winn, J. N., Vanderspek, R., et al. 2015, JATIS, 1, 014003
Royer, F., Grenier, S., Baylac, M. O., Gómez, A. E., & Zorec, J. 2002, A&A, 393, 897R
Sharma, A. N., Bedding, T. R., Saio, H., & White, T. R. 2022, MNRAS, 515, 828S
Swihart, S. J., Garcia, E. V., Stassun, K. G., et al. 2017, AJ, 153, 16
van Leeuwen, F. 2007, A&A, 474, 653